Title:
Plasmonic Enhanced Polarization Insensitive Second Harmonic Generation from $NbOCl_2$

Author:
Ziyu Wang[a#], Omar Abdelrahman Mohamed Abdelraouf[a#], Ishika Das[b#], Ruihuan Duan[c], Zheng Liu[c], Patrick Parkinson[b*] and Hong Liu[a,c,d*]

[a] *Institute of Materials Research and Engineering (IMRE), Agency for Science, Technology and Research (A*STAR), 2 Fusionopolis Way, #08-03, Innovis, Singapore 138634, Singapore*
[b] *Department of Physics and Astronomy, University of Manchester, Manchester, United Kingdom*
[b] *School of Materials Science and Engineering, Nanyang Technological University, 50 Nanyang Avenue, Singapore 639798, Singapore*
[c] *Department of Materials Science and Engineering, National University of Singapore, 9 Engineering Drive 1, #03-09 EA, Singapore 117575, Singapore*

#These authors contributed equally
*Corresponding author: h-liu@a-star.edu.sg, patrick.parkinson@manchester.ac.uk

Abstract
The niobium oxide dihalide series, $NbOX_2$ (X = Cl, Br, I), exhibits remarkable second-order optical nonlinearity and distinctive polarization-dependent properties. These characteristics make $NbOX_2$ an exceptional platform for applications in electronics, optoelectronics, and quantum technologies. $NbOX_2$ enables highly efficient second harmonic generation (SHG), a key process for the realization of advanced optical devices such as frequency converters and coherent light sources. The nonlinear optical performance of $NbOCl_2$ can be further enhanced through integration with plasmonic architectures, which intensify light–matter interactions and boost SHG efficiency. Here, we present a polarization-independent plasmonic structure that achieves a three-fold enhancement in SHG intensity, providing a robust pathway toward high-performance, miniaturized nonlinear optical systems.

Introduction

Second-harmonic generation (SHG) is one of the most fundamental nonlinear optical (NLO) processes, serving as a cornerstone of modern photonics.[1] By coherently converting two photons of frequency ω into one photon of frequency 2ω, SHG enables frequency conversion[2], wavelength tuning[3], and coherent light generation[4] essential for applications in ultrafast spectroscopy, optical communications, quantum information processing, and biomedical imaging[5-10]. Over the past decades, SHG has been widely exploited in bulk nonlinear crystals, such as lithium niobate ($LiNbO_3$)[11] and potassium titanyl phosphate (KTP)[12], where phase-matching and quasi-phase-matching (QPM) techniques are typically required to overcome dispersion and maintain constructive interference between the fundamental and second-harmonic waves. These strategies have achieved conversion efficiencies up to several tens of percent, supporting the development of high-power laser systems and quantum optics platforms.[13, 14] However, due to the intrinsic three-dimensional (3D) geometry and fabrication challenges of conventional nonlinear crystals[15, 16], these approaches remain largely incompatible with nanoscale photonic devices and on-chip integration, motivating the exploration of alternative materials and design strategies. [17, 18]

The advent of two-dimensional (2D) van der Waals (vdW) materials has revolutionized the field of nonlinear optics by introducing a new route to atomically thin media with exceptionally large optical nonlinearities.[19-23] In such systems, broken inversion symmetry and strong excitonic effects contribute to remarkably high second-order susceptibilities ($\chi^{(2)}$), often exceeding traditional bulk crystals (*e.g.* $\chi_{22}^{(2)} \sim 4\ pm/v$ for beta-barium borate and $\chi_{33}^{(2)} \sim 60\ pm/v$ for lithium niobate)[24]. Furthermore, the facile integration of 2D materials with nanophotonic platforms paves the way for hybrid optoelectronic architectures, enabling diverse functionalities such as all-optical signal modulation, nanoscale frequency conversion, and optical sensing.[25, 26] Nonetheless, the limited optical interaction length in these ultrathin layers restricts the absolute SHG generation, resulting in intrinsically low conversion efficiencies that hinder their use in practical nonlinear optical devices.[27]

Among the wide family of 2D materials, layered niobium oxyhalides ($NbOX_2$, X = Cl, Br, I) have recently emerged as particularly promising candidates for efficient nonlinear photonics owing to their intrinsic ferroelectricity, strong in-plane anisotropy, and large second-order susceptibilities coefficients over $100\ pm/V$.[13, 14, 28, 29] The intrinsic monoclinic crystal structure breaks inversion symmetry, giving rise to a robust spontaneous in-plane polarization that persists even at atomically thin dimensions This yields robust SHG that scales with thickness, which is significantly different from widely studied 2D transition metal dichalcogenides (TMDs) such as MoS_2[30] and $MoSe_2$[31]. Recent theoretical analyses have revealed that the giant second-order response in $NbOX_2$ originates from double-photon resonances between occupied anion p orbitals and unoccupied Nb 4d orbitals, as well as band-nesting effects that enhance the joint density of states.[14, 28] Furthermore, the NLO properties of $NbOX_2$ are closely coupled to its ferroelectric polarization, enabling dynamic tunability *via* external strain, electric fields, or phase transitions between ferroelectric and paraelectric states.[29, 32] These combined features position $NbOX_2$ as an ideal 2D material platform for next-generation nonlinear and quantum photonic devices.

To enhance the nonlinear response of ultrathin material, several optical enhancement strategies have been developed. Recent experimental studies have demonstrated significant progress in improving the NLO performance of $NbOX_2$ through nanophotonic and cavity integration. For instance, the incorporation of $NbOCl_2$ into 1D photonic crystal microcavities has resulted in more than an order-of-magnitude SHG enhancement owing to the strong field confinement and the optical feedback provided by distributed Bragg reflectors.[27] The dielectric multilayer structure also serves as an encapsulation medium, protecting $NbOCl_2$ from ambient degradation and maintaining long-term stability of the nonlinear signal. In parallel, $NbOCl_2$ metasurfaces and nanodisk arrays have been engineered to support Mie-type resonances and high-refractive-index contrast, achieving up to 25× SHG enhancement and enabling resonant light confinement within subwavelength volumes.[33] Photonic crystal (PhC) cavities has also proven particularly effective for boosting SHG intensity.[13] These results

highlight the tremendous potential of optical structure engineering for enhancing the nonlinear response of 2D $NbOX_2$ materials.

Beyond cavity and metasurface approaches, phase-matching and stacking engineering in $NbOX_2$ systems have opened new possibilities for optimizing SHG output. Controlled stacking of $NbOBr_2$ flakes with reverse alignment enables the compensation of phase mismatch between the fundamental and second-harmonic fields, resulting in entangled photon pair generation enhancement and optimized coherence lengths in both reflection and transmission geometries.[34, 35] Such approaches demonstrate that artificial structural manipulation in 2D materials can mimic quasi-phase-matching techniques traditionally realized in bulk ferroelectrics. Despite these significant advances, most reported enhancement strategies rely on dielectric or photonic confinement, which typically provide moderate field localization. The exploration of plasmonic architectures however, remains relatively limited for $NbOX_2$ materials.

Plasmonic nanostructures can dramatically intensify local electromagnetic fields through collective oscillations of free electrons at metal-dielectric interfaces, creating "hot spots" where the electric field amplitude is enhanced by orders of magnitude. When coupled with nonlinear media, such as 2D semiconductors, these localized fields can strongly boost nonlinear polarization and thus SHG efficiency. Furthermore, by carefully designing the geometry and symmetry of plasmonic elements, it is possible to achieve polarization-independent resonances, ensuring isotropic field enhancement for both linear and circularly polarized excitation.[36] Compared to purely dielectric systems, plasmonic platforms offer broadband operation, tunable resonance frequencies, and compact device footprints, making them attractive for ultrafast and integrated nonlinear photonics. The integration of $NbOCl_2$ with plasmonic architectures thus represents a promising yet underexplored strategy for unlocking the full nonlinear potential of this material family. In addition to field enhancement, plasmonic systems can also facilitate energy confinement and phase control at the nanoscale, enabling efficient coupling of fundamental and harmonic fields. Such hybrid configurations are particularly advantageous for applications requiring low excitation powers and miniaturized geometries, where conventional cavity-based solutions may suffer from

alignment sensitivity or limited optical bandwidth. Furthermore, plasmonic integration is compatible with scalable fabrication techniques such as electron-beam lithography and nanoimprint patterning, paving the way toward wafer-scale production of nonlinear optical elements based on 2D materials.

In this work, we present a polarization-independent plasmonic architecture that achieves a three-fold enhancement in SHG intensity from $NbOCl_2$ thin films. By coupling $NbOCl_2$ with a carefully engineered plasmonic nanostructure, we exploit the strong local field amplification at the plasmonic resonance to boost the effective nonlinear polarization while maintaining isotropic optical response across all polarization states. This design circumvents the limitations of anisotropic or polarization-sensitive enhancement schemes reported previously in cavity or metasurface systems. Moreover, the broadband nature of the plasmonic resonance allows efficient excitation under varied illumination conditions, enabling robust SHG performance over a wide spectral range.

Our findings demonstrate that plasmonic–$NbOCl_2$ hybrid systems can serve as powerful platforms for miniaturized nonlinear optical devices, combining the intrinsic strong $\chi^{(2)}$ response of $NbOCl_2$ with the extreme field confinement of plasmonic nanostructures. The observed three-fold enhancement in SHG intensity establishes a new route toward high-performance, scalable, and polarization-insensitive nonlinear photonic components. Beyond the immediate enhancement of harmonic generation, the principles demonstrated here can be extended to other nonlinear processes, including sum-frequency generation, spontaneous parametric down-conversion, and third-harmonic generation. Overall, this work bridges the gap between the fundamental optical nonlinearity of 2D $NbOX_2$ materials and practical, integrable device architectures, opening promising avenues for the realization of next-generation chip-scale light sources, frequency converters, and quantum photonic systems.

Results and Discussion

We begin by characterizing the intrinsic nonlinear optical (NLO) response of $NbOCl_2$ before introducing plasmonic coupling. As shown in the SHG mapping of Figure 1a, the SHG emission varies systematically with flake thickness, spanning 15 - 45 nm. This trend arises from the cumulative buildup of nonlinear polarization $p^{(2)}$, which scales with the number of layers in ferroelectric $NbOX_2$ systems. Unlike transition metal dichalcogenides (TMDs), whose SHG often quenches beyond monolayer thicknesses due to inversion symmetry recovery, $NbOCl_2$ maintains a noncentrosymmetric structure independent of layer number which is an intrinsic advantage for scalable nonlinear devices over TMD materials. Raman spectroscopy (Figure 1b) confirms the structural integrity of the exfoliated crystals. Multiple high-frequency modes assigned to Nb-O stretching and Nb-Cl vibrations indicate strong intralayer bonding. Furthermore, the optical constants remained stable over a one-year recording period (Figure 1c), which underscore the environmental robustness of $NbOCl_2$. This ambient stability is particularly noteworthy given that many vdW halides (*e.g.,* CrI_3, $FeCl_2$) degrade within hours in air. Additionally, the distinct optical constants along different axes identify $NbOCl_2$ as a birefringent component; a detailed discussion of this optical anisotropy is provided in Figure S1 and Figure S2. Complementary structural characterization, including XRD, XPS, and TEM imaging, is presented in Figure S3. The structural resilience of $NbOCl_2$ makes it suitable for long-term photonic integration and real-world applications. The power-dependent SHG measurements (Figure 1d) show a quadratic dependence on excitation power, validating the process as pure second-harmonic generation without contributions from multiphoton photoluminescence or other higher-order effects. This clean nonlinear scaling is essential for quantitative comparison between bare and plasmonically enhanced configurations. Polarization-resolved SHG measurements (Figure 1e) reveal a pronounced anisotropy with a characteristic two-lobed pattern. This arises from the monoclinic lattice symmetry and in-plane ferroelectric orientation of $NbOCl_2$. Notably, the polarization axis of maximal SHG emission correlates with the direction of spontaneous polarization, consistent with theoretical predictions that the nonlinear susceptibility tensor elements are strongly

anisotropic. Such intrinsic anisotropy imposes limitations on device applications where polarization alignment is impractical，motivating our development of a polarization-insensitive plasmonic enhancement platform. Finally, wavelength-dependent SHG spectra (Figure 1f) collected under pump wavelengths ranging from 750–800 nm shows consistent harmonic peaks at the expected half-wavelength positions, demonstrating robust spectral conversion efficiency. The broad resonance tolerance of $NbOCl_2$ indicates that it is not restricted to narrowband excitation, making it compatible with real plasmonic resonator bandwidths. Together, these intrinsic measurements establish $NbOCl_2$ as a stable, high-performance nonlinear medium with strong second-order responses and motivate the pursuit of external field enhancement strategies to overcome the limited interaction volume inherent in ultrathin materials.

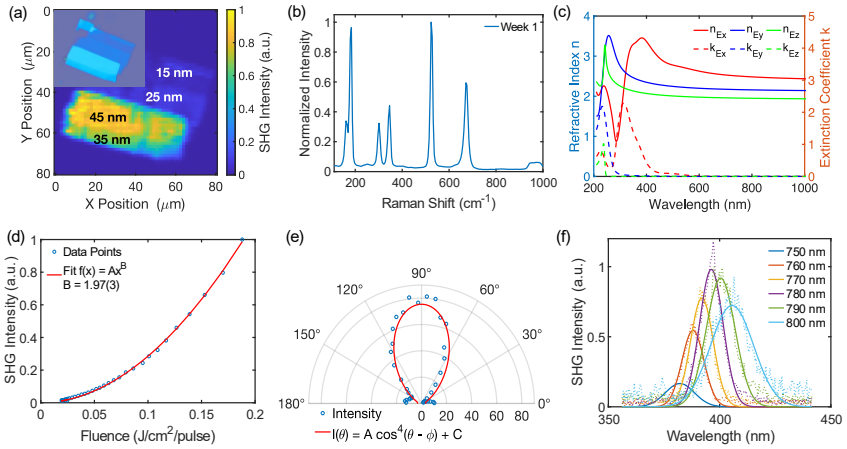

Figure 1 SHG measurement and Raman measurement of $NbOCl_2$ flakes. (a) SHG mapping of $NbOCl_2$ flakes with thicknesses of 15 - 45 nm under 780 nm excitation. Brighter regions correspond to stronger nonlinear emissions. (b) Raman spectra of $NbOCl_2$ flakes. (c) Optical constants for $NbOCl_2$ with thickness of 85 nm along three axis. (d) Power-dependent SHG intensity fitted to a quadratic function, confirming second-order nonlinear behavior. (e) Polarization-resolved SHG intensity exhibiting a characteristic anisotropic two-lobed pattern. (f) SHG spectra measured under pump wavelengths from 750 to 800 nm, with second harmonic peaks appearing at the expected half-wavelength positions.

To address the dual challenges of limited interaction length inherent to ultrathin 2D films and the intrinsic polarization constraints of the monoclinic $NbOCl_2$ crystal, we strategically engineered a plasmonic metasurface composed of C-4 symmetric Silver

(Ag) ring resonators. The device architecture is schematically illustrated in Figure 2a, depicting the integrated $NbOCl_2$ flake precisely positioned over the periodic array of resonators, the geometry of which was confirmed by SEM as shown in Figure 2b. We selected circular rings specifically for their in-plane symmetry. Unlike nanorods or bowtie antennas, which are inherently anisotropic and would bias the measurement, the ring's symmetric geometry ensures that the observed anisotropy originates solely from the $NbOCl_2$. In stark contrast, the rotational symmetry of the ring structure is meticulously designed to support plasmonic modes that can be excited efficiently by any in-plane polarization angle, thus ensuring a polarization-insensitive coupling mechanism. The underlying mechanism of enhancement was thoroughly investigated using Finite-Difference Time-Domain (FDTD) simulations. As demonstrated in Figure 2c, these simulations clearly elucidate the formation of a continuous, radially uniform "hotzone" along both the inner and outer edges of the Ag rings, rather than just at localized tips or gaps typical of gapped structures. Within these sub-wavelength volumes, the local electric field intensity ($|E_{loc}|^2$) is amplified by one order of magnitude relative to the incident field ($|E_{in}|^2$). Since the intensity of the second-harmonic signal scales with the fourth power of the fundamental field $I_{SHG} \propto |E_{loc}(\omega)|^4$, even moderate plasmonic confinement translates into a dramatic amplification of the nonlinear yield. The efficacy of this polarization-insensitive design was experimentally verified through transmission spectra measurements, presented in Figure 2d. The transmission spectra obtained under both linear and circular excitations exhibit indistinguishable resonance profiles. This observation explicitly validates the polarization-insensitive nature of the plasmonic resonance, confirming that the ring structure functions exclusively as a scalar field amplifier. This localized field concentration not only efficiently addresses the poor light-matter interaction volume typical of few-layer 2D materials but also maximizes the utilization of the material's intrinsically large nonlinear susceptibility, validating the ring-based metasurface as an effective platform for ultra-efficient, polarization-preserving frequency conversion. The novelty lies precisely in this ability to decouple the enhancement magnitude from the polarization response, ensuring the measured SHG is a faithful, yet amplified, representation of the material's intrinsic ferroelectric

Commented [PP1]: How many? Two?

anisotropy.

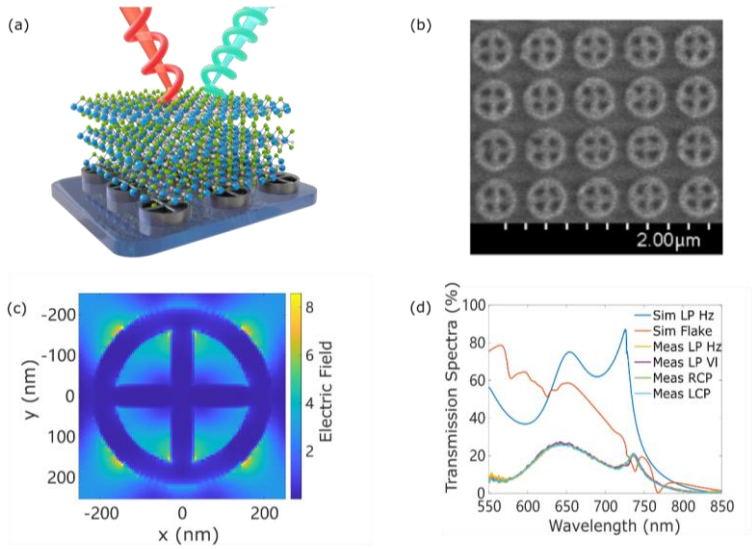

Figure 2. (a) Schematic of the C4-symmetric plasmonic resonator used for SHG enhancement. (b) SEM image of the fabricated resonator array showing uniform circular ring geometry. (c) Simulated local electric-field distribution revealing strong hotspot formation at the ring edges. (d) Measured transmission spectra under linear (Hz/Vl) and circular (RCP/LCP) polarizations, demonstrating polarization-insensitive plasmonic resonance.

The successful integration of $NbOCl_2$ flakes with engineered plasmonic architectures yields a substantial enhancement in nonlinear optical performance, effectively bridging the gap between intrinsic material properties and device-level efficiency. The schematic configuration of the experimental setup used for these measurements is illustrated in Figure 3d. As demonstrated by the spatial SHG mapping in Figure 3a, the hybrid system exhibits distinct optical contrast that clearly differentiates the substrate, the pristine bare flake, and the plasmonic-coupled regions (designated as Points A, B, and C, respectively). This spatial fidelity confirms that the optical enhancement is strictly confined to the light-matter interface rather than resulting from bulk measurement artifacts.

Quantitative analysis provided by the SHG line profile in Figure 3b further elucidates this behavior, revealing a pronounced amplification of approximately three-fold in SHG intensity (highlighted by the shaded region). This enhancement is specifically localized to the spatial overlap between the $NbOCl_2$ flake and the underlying plasmonic resonators, underscoring the efficacy of the electromagnetic 'hot spots' at the ring edges in boosting the effective nonlinear polarization. The polarization-resolved dynamics presented in Figure 3c reveal the preservation of symmetry within the hybrid system. In contrast to conventional plasmonic antennas, such as nanorods or bowties, where geometric anisotropy dictates the polarization response, our C_4-symmetric ring geometry strictly preserves the intrinsic anisotropic SHG signature of the $NbOCl_2$ crystal. The rotationally symmetric near-field distribution facilitates uniform amplification of all in-plane excitation vectors, effectively functioning as a scalar amplification factor. Consequently, the signal magnitude is enhanced without perturbing the angular emission pattern governed by the nonlinear susceptibility tensor. This decoupling of field enhancement from polarization distortion is critical for tensor-resolved nonlinear photonics, as it retains crystallographic orientation information without the artificial distortions typically associated with anisotropic metallic resonators

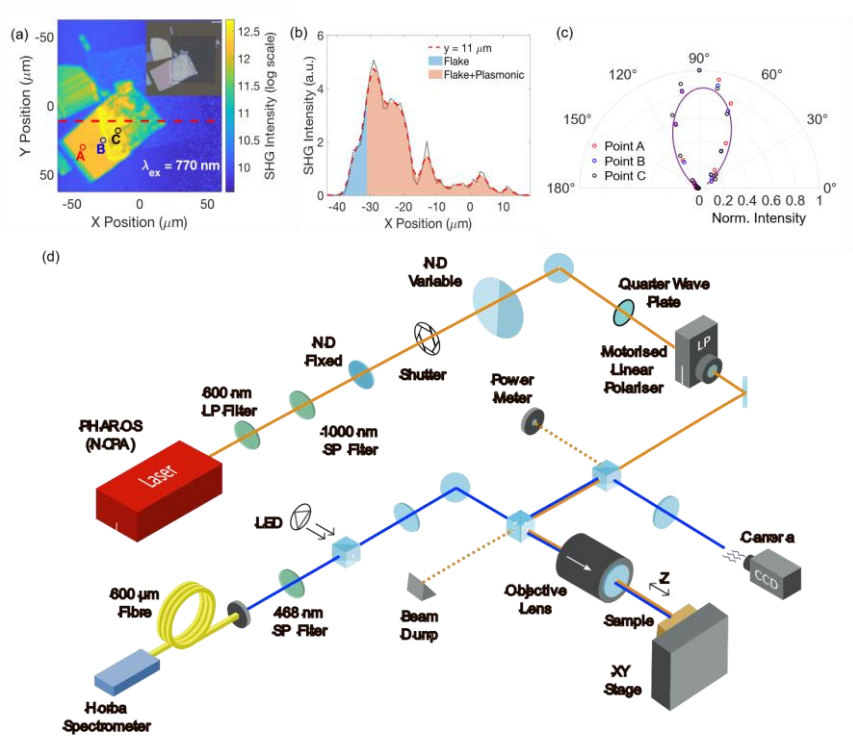

Figure 3. (a) Spatial SHG map of a $NbOCl_2$ flake transferred onto the plasmonic resonator array (λ_{ex} = 770 nm). Points A, B, and C indicate representative locations across the bare flake, plasmonic edge and plasmonic–flake hybrid regions. (b) SHG line profile extracted along the dashed line in (a), showing distinct regions corresponding to the bare flake and plasmonic–flake hybrid region. A pronounced increase in SHG intensity is observed when the flake overlaps with the plasmonic resonators, highlighting plasmon-assisted field enhancement. (c) Normalised polarization-resolved SHG intensities collected at points A, B and C shown in (a). The bare flake displays the characteristic two-lobed anisotropic emission pattern of $NbOCl_2$. In contrast, the plasmonically coupled region exhibits a well-preserved SHG pattern that retains the intrinsic anisotropy of $NbOCl_2$ under the influence of the C_4-symmetric plasmonic field distribution. (d) Schematic illustration of the experimental setup for SHG measurements in reflection mode.

To rigorously evaluate the optical stability and thermal dissipation mechanisms of the $NbOCl_2$ material system, we conducted comparative damage threshold tests on both substrate-supported and suspended geometries. Figure 4a presents optical micrographs of a representative $NbOCl_2$ flake with a thickness of 450 nm on a Si/SiO_2 substrate, while Figure 4b depicts a flake suspended over pre-patterned trenches, serving as a control

sample isolated from substrate interactions. The corresponding power dependent SHG response is detailed in Figure 4c. In the low-fluence regime, both the substrate-supported (blue) and suspended (red) samples exhibit a strict quadratic dependence on excitation power, unambiguously confirming the second-order nature of the nonlinear process. However, a distinct divergence in performance emerges at higher excitation intensities. The suspended flake exhibits nonlinear saturation at a lower fluence threshold of 0.69 ± 0.01 J/cm^2/pulse, compared to its supported counterpart at 0.78 ± 0.04 J/cm^2/pulse. This premature saturation is attributed to the thermal isolation of the suspended membrane; lacking the substrate to act as a conductive heat sink, the flake experiences reduced heat dissipation and rapid thermal accumulation. This comparison highlights the critical role of the substrate in managing thermal load and extending the operational dynamic range of the nonlinear device.

Commented [PP2]: This is true. However, it would be good to report the actual damage threshold as I believe that it is significantly higher than literature values for comparable materials. Ishika – please can you add?

The reported laser-induced damage thresholds for bulk nonlinear crystals such as β-BBO under near-infrared excitation and sub-picosecond pulse durations are typically on the order of tens of GW cm^{-2}, corresponding to fluences of ~10^{-2} J/cm²/pulse.[37] While a fully quantitative comparison would require measurements performed under identical excitation conditions on both materials, such literature values nevertheless indicate that $NbOCl_2$ exhibits a markedly higher tolerance to intense ultrafast optical excitation. This robustness, together with its strong nonlinear response, underscores the potential of $NbOCl_2$ for device-level nonlinear photonic applications operating at high optical fluences.

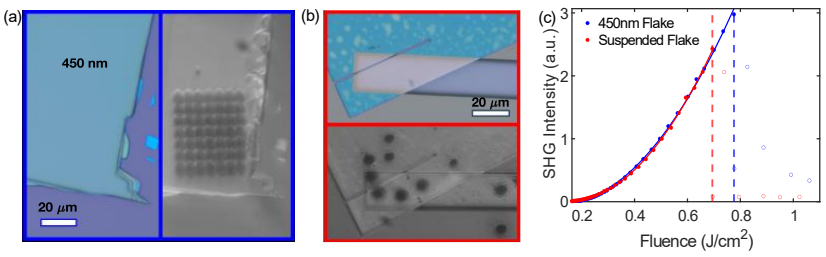

Figure 4. Thermal stability and saturation thresholds of $NbOCl_2$. (a) Optical micrographs of a $NbOCl_2$ flake with a thickness of 450 nm on a Si/SiO_2 substrate prior to laser damage testing. (b) Optical micrographs of a suspended $NbOCl_2$ flake bridging a pre-patterned trench, serving as a thermally isolated control. (c) Power-dependent SHG intensity for the substrate-supported (blue) and suspended (red) configurations. Both datasets initially exhibit quadratic power dependence (solid lines), confirming the second-order nonlinear origin. The suspended flake saturates at a noticeably lower fluence threshold than the supported sample, indicating that the substrate is essential for effective heat dissipation and maintaining linear operation at high powers.

Conclusion

In summary, we have demonstrated a polarization-insensitive plasmonic enhancement strategy that significantly amplifies the intrinsic second-harmonic generation of $NbOCl_2$, a highly nonlinear and air-stable van der Waals ferroelectric. By integrating $NbOCl_2$ flakes with C_4-symmetric circular Ag resonators, we achieve approximately three-fold enhancement in SHG intensity, enabled by strong near-field confinement and broadband plasmonic resonance that overlaps the excitation wavelength. This polarization-independent behavior arises from the rotational symmetry of the resonators, which dominates the local electromagnetic environment and homogenize the angular distribution of the nonlinear polarization.

The hybrid platform presented here addresses key challenges in applying anisotropic 2D ferroelectrics to practical nonlinear photonic architectures, including sensitivity to crystal orientation and polarization alignment. The compatibility of the plasmonic resonators with broadband excitation, their fabrication scalability, and their robust enhancement behavior collectively highlight the potential of plasmonic / vdW integration for compact frequency converters, ultralow-power coherent light sources, polarization-agnostic nonlinear modules, and quantum-optical applications. Given the strong $\chi^{(2)}$ response and ferroelectric tunability of $NbOX_2$ materials, future work may explore electrically modulated SHG, nonlinear phase shaping, and plasmon-assisted entangled photon generation. Overall, this study establishes a versatile approach for boosting nonlinear optical responses in atomically thin ferroelectrics and advances the development of high-performance, chip-scale nonlinear photonic systems.

Method

FDTD Optical Simulations and Field Analysis

A three-dimensional finite-difference time-domain computational approach (Lumerical FDTD Solutions) was employed to simulate the optical behavior of the plasmonic metasurface. Material parameters for silver and quartz were sourced from experimental ellipsometry measurements and incorporated into the simulation framework. The structure was subjected to a linearly polarized electromagnetic wave oriented along the x-axis, with boundary conditions configured to allow periodic repetition in the transverse

(x–y) plane and absorbing boundary layers (perfectly matched layers) extending vertically (z-axis) to suppress outgoing radiation and prevent spurious reflections. Spatial discretization was maintained at 5 nm or smaller to guarantee computational accuracy. Field distribution data was collected at two strategic locations: beneath the quartz interface to measure transmitted intensity, and at the center height of the silver nanostructure to resolve electromagnetic field patterns corresponding to plasmonic resonance conditions. Convergence was verified using an auto-shutoff criterion set at 5×10^{-7}, ensuring reliable and precise numerical results.

Experimental Transmission Characterization

Optical transmission properties were investigated using a pulsed broadband laser system (Opera model from Leukos Laser Inc.) operating at 30 kHz pulse repetition frequency. The incident illumination was linearly polarized in the *x*-direction using a polarization management system incorporating a quarter-wave retarder, half-wave retarder, and sheet polarizer, allowing selective excitation of the plasmonic metasurface resonance. The transmitted light was collected, coupled into an optical fiber, and directed toward a spectrometer (Ocean Optics USB4000) connected to a data acquisition interface for spectral recording and analysis.

Metasurface Nanofabrication and Patterning Process

Fabrication of a polarization-independent plasmonic metasurface operating in the visible wavelength range began with substrate preparation. Double-sided polished transparent deep-UV quartz plates (from Photonik Singapore) were sequentially rinsed with acetone and isopropanol, then ultrasonically cleaned for 10 minutes in acetone, followed by final rinses with organic solvents and nitrogen drying. A 100 nm silver film was applied to the prepared substrate via electron beam evaporation (Denton Explorer instrument). Nanoscale patterning was achieved through electron beam lithography (Elionix ELS-7000), wherein a 6% hydrogen silsesquioxane photoresist was applied at 2000 rpm rotation for 60 seconds, followed by a charging mitigation layer (EZspacer) deposited at 1500 rpm for 30 seconds and subsequently dried with nitrogen. The patterning process utilized specialized dose-correction algorithms (Beamer software) to compensate for proximity effects and backscatter, employing a 500 pA electron beam at 100 kV

operating voltage with base dose of 13,000 μC/cm² over a 300×300 μm² region encompassing 60,000 exposure locations. Pattern development commenced with charging-layer removal through deionized water rinsing and nitrogen drying, followed by a 60-second immersion in alkaline developer solution (25% NaOH/NaCl mixture), then stopped by immersion in deionized water for 60 seconds, with final rinsing in fresh deionized water and isopropanol and nitrogen drying. Transfer of the patterned template to the silver layer was performed using inert gas ion dry etching (Oxford Ionfab300Plus, CAIBE mode) with argon gas (22 sccm) at 600 V bias voltage, 5 mTorr chamber pressure, and ambient temperature, achieving a silver removal rate of approximately 40 nm/min and eliminating residual HSQ mask.

Nonlinear Optical Characterization

Second-harmonic generation (SHG) measurements were carried out using a femtosecond pulsed laser operating in the near-infrared spectral range (750–800 nm) at a repetition rate of 100 kHz, with pulse durations of approximately 250 fs. The incident beam was passed through a half-wave plate and linear polarizer to control the excitation polarization and focused onto the sample using a 20× objective lens with a numerical aperture of 0.75, producing a laser spot diameter of approximately 2 μm. The generated SHG signal was collected in a reflection geometry using the same objective, spectrally filtered to remove the fundamental wavelength, and detected using a fibre-coupled spectrometer. Power-dependent SHG spectra were acquired by incrementally increasing the incident average power while keeping all other acquisition parameters constant. The SHG intensity was obtained by integrating the spectral peak at the second-harmonic wavelength.

Laser-induced damage measurements were performed by monitoring deviations from the expected quadratic dependence of SHG intensity on excitation fluence. The fluence was calculated from the measured average power, laser repetition rate, and focal spot area. Measurements were repeated across multiple spatial locations and for both supported and suspended flakes to ensure reproducibility. The damage threshold was defined as the fluence at which an irreversible deviation from quadratic SHG scaling was observed.

Conflicts of interest

There are no conflicts to declare.

Acknowledgment

H. Liu and Z. Liu acknowledge the support from National Research Foundation Competitive Research Programme (CRP) funding of Singapore under award no. NRF-CRP31-0001 and the RIE2025 Manufacturing, Trade and Connectivity (MTC) Programmatic Fund (M23M2b0056). H. Liu acknowledges RIE2025 MTC Individual Research Grants (IRG) (M24N7c0087). Z. Liu acknowledges supports from Singapore National Research Foundation–Competitive Research Program NRF-CRP22-2019-0007, and NRF-CRP264-2021-0004. This research is also supported by the Singapore Ministry of Education Tier 3 and Tier 2 Programmatic Fund (award no. MOEMOET32023-0003, and MOE-T2EP50223-0008) and the Singapore Ministry of Education Academic Research Fund (AcRF) Tier 1 (award no. 023785-00001). R. Duan acknowledges support from the Agency for Science, Technology and Research (A*STAR) under the MTC Young Individual Research Grants (YIRG) (M24N8c0097). P. Parkinson and I. Das acknowledges support from UKRI through the Future Leaders Fellowship Renewal under grant number MR/Y03421X/1.

Reference

[1] Maker, P. D.; Terhune, R. W.; Nisenoff, M.; Savage, C. M. Effects of Dispersion and Focusing on the Production of Optical Harmonics. *Phys. Rev. Lett.* **1962**, *8*, 21.

[2] Konforty, N.; Cohen, M.-I.; Segal, O.; Plotnik, Y.; Shalaev, V. M.; Segev, M. Second harmonic generation and nonlinear frequency conversion in photonic time-crystals. *Light Sci. Appl.* **2025**, *14*, 152.

[3] Yuan, Z.; Ge, J.; Liu, P.; Li, B.; Li, M.; Liu, J. Y.; Yu, Y.; Chen, H. J.; Bowers, J.; Vahala, K. Efficient and wavelength-tunable second-harmonic generation toward the green gap. *Sci. Adv.* **2025**, *11*, eadw2781.

[4] Billat, A.; Grassani, D.; Pfeiffer, M. H. P.; Kharitonov, S.; Kippenberg, T. J.; Brès, C.-S. Large second harmonic generation enhancement in Si3N4 waveguides by all-optically induced quasi-phase-matching. *Nat. Commun.* **2017**, *8*, 1016.

[5] Ma, J.; Ren, J.; Zhang, J.; Meng, J.; McManus-Barrett, C.; Crozier, K. B.; Sukhorukov, A. A. Quantum imaging using spatially entangled photon pairs from a nonlinear metasurface. *eLight* **2025**, *5*, 2.

[6] Zipfel, W. R.; Williams, R. M.; Webb, W. W. Nonlinear magic: multiphoton microscopy in the biosciences. *Nat. Biotechnol.* **2003**, *21*, 1369.

[7] Zhao, J.; Fieramosca, A.; Bao, R.; Du, W.; Dini, K.; Su, R.; Feng, J.; Luo, Y.; Sanvitto, D.; Liew, T. C. H.; et al. Nonlinear polariton parametric emission in an atomically thin semiconductor based microcavity. *Nat. Nanotechnol.* **2022**, *17*, 396.

[8] Hickstein, D. D.; Carlson, D. R.; Mundoor, H.; Khurgin, J. B.; Srinivasan, K.; Westly, D.; Kowligy, A.; Smalyukh, I. I.; Diddams, S. A.; Papp, S. B. Self-organized nonlinear gratings for ultrafast nanophotonics. *Nat. Photonics* **2019**, *13*, 494.

[9] Tognazzi, A.; Franceschini, P.; Biechteler, J.; Baù, E.; Cino, A. C.; Tittl, A.; De Angelis, C.; Sortino, L. Interface second harmonic generation enhancement in bulk WS2/MoS2 hetero-bilayer van der Waals nanoantennas. *Light Sci. Appl.* **2025**, *14*, 346.

[10] Lin, K.-Q.; Bange, S.; Lupton, J. M. Quantum interference in second-harmonic generation from monolayer WSe2. *Nat. Phys.* **2019**, *15*, 242.

[11] Tang, Y.; Ding, T.; Zhang, Y.; Ding, W.; Huang, Y.; Wang, J.; Li, H.; Liu, S.; Zheng, Y.; Chen, X. Octave-Spanning Second-Harmonic Generation in Dispersion-Engineered Lithium Niobate-on-Insulator Microwaveguide. *Adv. Photonics Res.* **2024**, *5*, 2400051.

[12] Zhang, S.; Yao, J.; Liu, W.; Huang, Z.; Wang, J.; Li, Y.; Tu, C.; Lu, F. Second harmonic generation of periodically poled potassium titanyl phosphate waveguide using femtosecond laser pulses. *Opt. Express* **2008**, *16*, 14180.

[13] Bai, L.; Jiang, M.; Qu, L.; Zhu, P.; Wu, W.; Li, Q.; Guo, Z.; Sun, X.; Huang, Z.; Xie, M.; et al. Photonic Crystal Defect Cavities Enable Air-Stable and Enhanced SHG from NbOCl2. *Adv. Opt. Mater.* **2025**, *13*, e01588.

[14] Guo, Q.; Qi, X.-Z.; Zhang, L.; Gao, M.; Hu, S.; Zhou, W.; Zang, W.; Zhao, X.; Wang, J.; Yan, B.; et al. Ultrathin quantum light source with van der Waals NbOCl2 crystal. *Nature* **2023**, *613*, 53.

[15] Wen, Y.; Chen, H.; Wu, Z.; Li, W.; Zhang, Y. Fabrication and photonic applications of Si-integrated $LiNbO_3$ and $BaTiO_3$ ferroelectric thin films. *APL Mater.* **2024**, *12*.

[16] Li, Z.; Wang, R. N.; Lihachev, G.; Zhang, J.; Tan, Z.; Churaev, M.; Kuznetsov, N.; Siddharth, A.; Bereyhi, M. J.; Riemensberger, J.; et al. High density lithium niobate photonic integrated circuits. *Nat. Commun.* **2023**, *14*, 4856.
[17] Geler-Kremer, J.; Eltes, F.; Stark, P.; Stark, D.; Caimi, D.; Siegwart, H.; Jan Offrein, B.; Fompeyrine, J.; Abel, S. A ferroelectric multilevel non-volatile photonic phase shifter. *Nat. Photonics* **2022**, *16*, 491.
[18] Gu, T.; Petrone, N.; McMillan, J. F.; van der Zande, A.; Yu, M.; Lo, G. Q.; Kwong, D. L.; Hone, J.; Wong, C. W. Regenerative oscillation and four-wave mixing in graphene optoelectronics. *Nat. Photonics* **2012**, *6*, 554.
[19] Di Gaspare, A.; Ghayeb Zamharir, S.; Knox, C.; Yagmur, A.; Sasaki, S.; Salih, M.; Li, L.; Linfield, E. H.; Freeman, J.; Vitiello, M. S. Second and third harmonic generation in topological insulator-based van der Waals metamaterials. *Light Sci. Appl.* **2025**, *14*, 337.
[20] Sun, Z.; Yi, Y.; Song, T.; Clark, G.; Huang, B.; Shan, Y.; Wu, S.; Huang, D.; Gao, C.; Chen, Z.; et al. Giant nonreciprocal second-harmonic generation from antiferromagnetic bilayer CrI3. *Nature* **2019**, *572*, 497.
[21] Yu, J.; Kuang, X.; Li, J.; Zhong, J.; Zeng, C.; Cao, L.; Liu, Z.; Zeng, Z.; Luo, Z.; He, T.; et al. Giant nonlinear optical activity in two-dimensional palladium diselenide. *Nat. Commun.* **2021**, *12*, 1083.
[22] Soavi, G.; Wang, G.; Rostami, H.; Purdie, D. G.; De Fazio, D.; Ma, T.; Luo, B.; Wang, J.; Ott, A. K.; Yoon, D.; et al. Broadband, electrically tunable third-harmonic generation in graphene. *Nat. Nanotechnol.* **2018**, *13*, 583.
[23] Du, L.; Hasan, T.; Castellanos-Gomez, A.; Liu, G.-B.; Yao, Y.; Lau, C. N.; Sun, Z. Engineering symmetry breaking in 2D layered materials. *Nat. Rev. Phys.* **2021**, *3*, 193.
[24] Zhou, B.; Kang, J. H.; Hu, B.; Zhou, J.; Ren, H.; Zhou, J.; Zhang, D.; Zhang, A.; Zheng, S.; Wong, C. W.; et al. Giant second harmonic generation in bulk monolayer MoS_2 thin films. *Matter* **2024**, *7*, 2448.
[25] Wang, Y.; Xiao, J.; Yang, S.; Wang, Y.; Zhang, X. Second harmonic generation spectroscopy on two-dimensional materials [Invited]. *Opt. Mater. Express* **2019**, *9*, 1136.
[26] Seidt, L.; Weber, T.; Seredin, A. A.; Possmayer, T.; Savelev, R.; Petrov, M. I.; Maier, S. A.; Tittl, A.; Menezes, L. d. S.; Sortino, L. Ultrafast all-optical switching in nonlinear 3R-MoS2 van der Waals metasurfaces. *npj Nanophotonics* **2025**, *2*, 37.
[27] Chen, W.; Zhu, S.; Duan, R.; Wang, C.; Wang, F.; Wu, Y.; Dai, M.; Cui, J.; Chae, S. H.; Li, Z.; et al. Extraordinary Enhancement of Nonlinear Optical Interaction in NbOBr(2) Microcavities. *Adv. Mater.* **2024**, *36*, e2400858.
[28] Abdelwahab, I.; Tilmann, B.; Wu, Y.; Giovanni, D.; Verzhbitskiy, I.; Zhu, M.; Berté, R.; Xuan, F.; Menezes, L. d. S.; Eda, G.; et al. Giant second-harmonic generation in ferroelectric NbOI2. *Nat. Photonics* **2022**, *16*, 644.
[29] Wang, Y.; Hossain, M. S.; Li, T.; Xiong, Y.; Le, C.; Kuebler, J.; Raghavan, N.; Fernandez-Ballester, L.; Hong, X.; Sinitskii, A.; et al. Ultrafast dynamics of ferroelectric polarization of NbOI2 captured with femtosecond electron diffraction. *Nat. Commun.* **2025**, *16*, 8132.

[30] Zhang, M.; Han, N.; Zhang, J.; Wang, J.; Chen, X.; Zhao, J.; Gan, X. Emergent second-harmonic generation in van der Waals heterostructure of bilayer MoS(2) and monolayer graphene. *Sci Adv* **2023**, *9*, eadf4571.
[31] Chen, H.; Corboliou, V.; Solntsev, A. S.; Choi, D.-Y.; Vincenti, M. A.; de Ceglia, D.; de Angelis, C.; Lu, Y.; Neshev, D. N. Enhanced second-harmonic generation from two-dimensional MoSe2 on a silicon waveguide. *Light Sci. Appl.* **2017**, *6*, e17060.
[32] Li, Z.; Wang, S.; Wang, C.; Zhang, X.; Yu, Z.; Du, S.; Zeng, Z.; Dai, Y.; Zhang, Y.; Liu, X.; et al. Peierls Distortion Induced Giant Linear Dichroism, Second-Harmonic Generation, and In-Plane Ferroelectricity in NbOBr2. *Small* **2025**, *21*, 2407729.
[33] Chu, L.; Gao, S.; Li, Z.; Zhu, H.; Liu, W.; Jia, Y.; Chen, F. van der Waals NbOCl2 Nanodisks for Enhanced Second-Harmonic Generation. *Nano Lett.* **2024**, *24*, 15457.
[34] Kallioniemi, L.; Lyu, X.; He, R.; Rasmita, A.; Duan, R.; Liu, Z.; Gao, W. Van der Waals engineering for quantum-entangled photon generation. *Nat. Photonics* **2025**, *19*, 142.
[35] Lyu, X.; Kallioniemi, L.; Hong, H.; Qu, R.; Zhang, Y.; Zúñiga-Perez, J.; Liu, K.; Gao, W. A tunable entangled photon-pair source based on a Van der Waals insulator. *Nat. Commun.* **2025**, *16*, 1899.
[36] Yu, H.; Peng, Y.; Yang, Y.; Li, Z.-Y. Plasmon-enhanced light–matter interactions and applications. *npj Comput. Mater.* **2019**, *5*, 45.
[37] Turčičová, H.; Novák, O.; Muzik, J.; Štěpánková, D.; Smrž, M.; Mocek, T. *Laser induced damage threshold (LIDT) of β-barium borate (BBO) and cesium lithium borate (CLBO) – Overview*. **Opt. Laser Technol. 2022**, *149*, 107876.